Research Square

Preprints are preliminary reports that have not undergone peer review.
They should not be considered conclusive, used to inform clinical practice,
or referenced by the media as validated information.

Early regional myocardial mechanics anticipate fibrosis extension after myocardial infarction

Gregory Franck

gregory.franck@inserm.fr

Université Paris Cité and Université Sorbonne Paris Nord, INSERM, LVTS https://orcid.org/0000-0002-4288-9034

Nolan Perlin

Université Paris Cité and Université Sorbonne Paris Nord, INSERM, LVTS

Tania Dubois-Mignon

Université Paris Cité and Université Sorbonne Paris Nord, INSERM, LVTS

Varouna Syvannarath

Université Paris Cité and Université Sorbonne Paris Nord, INSERM, LVTS

Younès Youssfi

Université Paris Cité and Université Sorbonne Paris Nord, INSERM, LVTS

Marylou Para

Université Paris Cité and Université Sorbonne Paris Nord, INSERM, LVTS

Sofiane Mohamed

Université Paris Cité and Université Sorbonne Paris Nord, INSERM, LVTS

Elnaz Ghajar-Rahimi

Weldon School of Biomedical Engineering, Purdue University

Laura Martinez Galindo

Weldon School of Biomedical Engineering, Purdue University

Sylvain Richard

PhyMedExp, Université de Montpellier, INSERM

Craig Goergen

Weldon School of Biomedical Engineering, Purdue University

Pierre Sicard

PhyMedExp, Université de Montpellier, INSERM

Antonino Nicoletti

INSERM

Giuseppina Caligiuri

Université Paris Cité and Université Sorbonne Paris Nord, INSERM, LVTS

Article

Keywords: myocardial infarction, regional mechanics, echocardiography, fibrosis, machine learning, spatial transcriptomics

Posted Date: November 20th, 2026

DOI: https://doi.org/10.21203/rs.3.rs-11801893/v1

License: This work is licensed under a Creative Commons Attribution 4.0 International License. Read Full License

Additional Declarations: There is **NO** Competing Interest.

Early regional myocardial mechanics anticipate fibrosis extension after myocardial infarction

Nolan Perlin [*1], Tania Dubois-Mignon [*1], Varouna Syvannarath [*1], Younès Youssfi [1], Marylou Para [1], Sofiane Mohamed [1], Elnaz Ghajar-Rahimi [2], Laura F. Martinez Galindo [2,3], Sylvain Richard [4], Craig J. Goergen [3], Pierre Sicard [4], Antonino Nicoletti [1], Giuseppina Caligiuri [§1], Grégory Franck [§1]

1. Université Paris Cité and Université Sorbonne Paris Nord, INSERM, LVTS, F-75018 Paris, France.
2. Weldon School of Biomedical Engineering, Purdue University, West Lafayette, Indiana, USA.
3. Department of Biomedical Engineering, Universidad de los Andes, Bogota, Colombia.
4. PhyMedExp, Université de Montpellier, INSERM, CNRS, Montpellier, France.

*These authors contributed equally. §These authors jointly supervised this work.

Corresponding author: Grégory Franck, Université Paris Cité and Université Sorbonne Paris Nord, INSERM, LVTS, F-75018 Paris, France; gregory.franck@inserm.fr

Graphical abstract

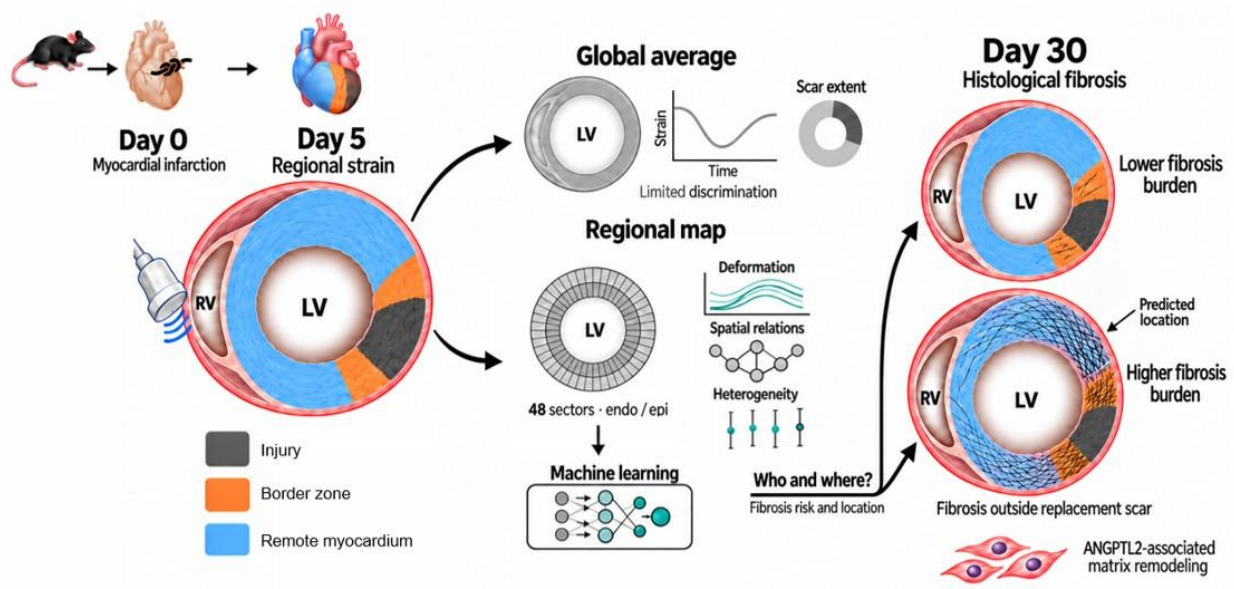

Abstract

Fibrosis after myocardial infarction extends beyond the replacement scar, but identifying hearts at risk of this later remodeling remains challenging. Here we investigate whether early regional myocardial mechanics anticipates fibrosis outside scar. In 35 mice from three cohorts undergoing permanent coronary ligation, day-5 echocardiographic mechanics were mapped to day-30 histology across 48 myocardial regions. Myocardial territories were defined from day-5 mechanics independently of later histology. When each mouse was held out in turn, physiologically summarized regional mechanics discriminated high fibrosis burden outside scar with an area under the receiver operating characteristic curve of 0.732, compared with 0.513 for globally averaged mechanics. In an exploratory analysis, adding the regional score to early scar extent, ejection fraction and global circumferential strain increased this value from 0.454 to 0.683 (difference, 0.229; 95% confidence interval, 0.086-0.392). Models trained directly on the complete deformation signals showed lower observed discrimination on the same mouse-level task. Whole-heart mapping and spatial transcriptomics extended the analysis across the ventricle and placed the imaging result within the later tissue-remodeling response. These findings support early regional mechanics as a source of information about subsequent fibrosis beyond conventional measures of ventricular injury and function.

Keywords: myocardial infarction; regional mechanics; echocardiography; fibrosis; machine learning; spatial transcriptomics

Introduction

Left-ventricular remodeling after myocardial infarction reflects both the initial loss of myocardium and the subsequent response of the surviving ventricular wall. Infarct size is an important determinant of later ventricular dilation and dysfunction [1]. However, tissue remodeling beyond the infarct also carries prognostic information as fibrosis in remote myocardium associates with heart-failure hospitalization and mortality, while being only weakly related to infarct size [9]. Identifying early signs of this later fibrotic remodeling could therefore complement assessment of the initial injury.

The biological significance of fibrosis depends on where it develops. Within the infarct, activated fibroblasts replace lost cardiomyocytes with extracellular matrix, forming the scar that supports the injured ventricular wall [6]. Beyond this replacement scar, the surviving myocardium undergoes a distinct remodeling response. Experimental studies show that fibroblast activation can extend throughout the

ventricle while collagen deposition remains spatially heterogeneous [8]. Together with the clinical association between remote fibrosis and adverse outcomes [9], these observations make fibrosis outside replacement scar a relevant target for early risk assessment.

Myocardial deformation offers a way to investigate this response through tissue function. Clinical studies have linked early mechanical dyssynchrony to subsequent ventricular remodeling and shown that regional strain abnormalities carry prognostic information even when conventional wall-motion assessment appears normal [3,5]. There is also a biological basis for examining local mechanics: mechanical destabilization can induce border-zone transcriptional programs, and stretch and matrix stiffness influence fibroblast activation and extracellular-matrix production [11,13]. These findings motivate the hypothesis that regional deformation reflects aspects of the tissue environment relevant to later fibrosis. Whether early echocardiographic mechanics can anticipate fibrosis outside scar, beyond conventional measures of injury and ventricular function, is the question addressed here.

Regional deformation curves describe how myocardial motion evolves throughout the cardiac cycle. Their magnitude, timing, variability and relationships with neighboring regions can be summarized while retaining their location within the ventricle. This provides a way to test whether regional information contributes beyond a global average. We can also analyze the complete deformation curves directly. Fair comparison of these representations, however, requires the same biological outcome and the same animals to be held out during validation.

Here, we combined serial echocardiography with D30 histology in a mouse model of permanent coronary occlusion. Myocardial territories were defined from D5 radial mechanics independently of D30 histology. Using the mouse as the unit of validation, we tested whether summarized regional mechanics identified high later fibrosis burden outside scars and provided additional information to early scar extent, ejection fraction and global strain. We then compared these physiological summaries with models trained directly on the complete deformation curves. Whole-heart mapping examined the relationship across ventricular levels, and spatial transcriptomics explored the associated remodeling states. This framework links early functional imaging to the later tissue response of myocardium outside the infarct scar.

Methods

Study design and cohorts

We used a mouse model of permanent left anterior descending coronary artery ligation, with echocardiography performed at baseline (D0), D5 and D30 and terminal tissue analysis at D30. The paired short-axis analysis comprised 35 infarcted mice from three experimental cohorts generated in Paris and Montpellier. Four sham-operated mice provided descriptive reference data. The mouse was the independent biological unit: all regions from a given heart remained together in training, validation or testing partitions. We described late ventricular remodeling in the 32 infarcted mice with available D30 global longitudinal strain (GLS). A fixed D30 GLS threshold classified adaptive remodeling (GLS below -9%; n = 16) and heart failure-like remodeling (GLS of -9% or greater; n = 16). Three mice without D30 GLS remained unclassified for phenotype displays but were retained in the 35-mouse fibrosis-prediction cohort. This late classification was descriptive and did not define the early myocardial territories or the fibrosis outcome. Animal procedures were authorized under APAFIS #39803-2022112915461850 and #43480-2022112915461850 by the French Ministry of Higher Education and Research. C57BL/6 mice underwent permanent coronary ligation below the left atrial appendage under general anaesthesia; sham-operated mice underwent thoracotomy without ligation.

Echocardiography and regional deformation

Transthoracic echocardiography was performed with a Vevo 3100 system and an MX550D transducer (FUJIFILM VisualSonics). Standard short- and long-axis measurements included ventricular volumes, ejection fraction and global strain. For regional analysis, endocardial and epicardial contours were traced in a mid-ventricular short-axis cine loop and the myocardial circumference was divided into 48 equally spaced regions.

Individual cardiac cycles were aligned to end-diastolic and end-systolic landmarks and resampled over a normalized cardiac cycle. Up to three analyzable cycles were averaged to obtain one representative regional curve; when only one cycle was available, that cycle was retained unchanged. We considered six signal families were considered: strain, strain rate, displacement, velocity, shear and shear rate. Radial and circumferential components and endocardial and epicardial layers were retained where available.

Definition of myocardial territories

We defined myocardial territories from D5 mechanics without using D30 histology. For each region, the signed area under the radial-strain curve over the complete normalized cardiac cycle was averaged across analyzable cycles. Values were min-max normalized within each heart,

$z = (x - \min(x)) / (\max(x) - \min(x))$,

where the minimum and maximum were calculated across the 48 regions. Regions with $z < 0.10$ defined the mechanically impaired scar territory. For every contiguous scar block, the four nearest non-scar regions on either side were assigned to the border zone; the remaining regions were designated remote myocardium. Scar retained priority when neighborhoods overlapped. This operational definition describes severe early mechanical impairment and is not a direct anatomical measurement of infarct size. The unscaled D5 radial-strain integrals across all 48 sectors, together with per-heart summaries, are shown in Supplementary Fig. S7.

Histology, spatial correspondence and fibrosis outcomes

At D30, transverse myocardial sections corresponding to the short-axis imaging plane were stained with Sirius Red and digitized. A custom image-analysis workflow quantified fibrotic area in the common 48-region coordinate system, retaining endocardial and epicardial information where available. For each circumferential sector, the whole-wall fibrosis percentage was calculated as 100 times the combined fibrotic area divided by the combined myocardial tissue area of the endocardial and epicardial compartments. A sector was classified as fibrotic when this percentage was strictly greater than 10%; values of 10% or less were classified as non-fibrotic. For each mouse, fibrosis burden outside scar was calculated as the number of fibrotic sectors in the combined border and remote territories divided by the total number of evaluable sectors in these territories. The imaging and histology maps were oriented from the septal insertion landmark and the recorded orientation of each heart. Sector 1 was anchored at the septal landmark and numbering proceeded counterclockwise. The same anatomical convention was used throughout the short-axis and whole-heart analyses. The primary mouse-level outcome was high D30 fibrosis burden outside scar, defined relative to the study cohort. For each mouse, burden was the proportion of fibrotic sectors in the combined border and remote territories. Mice with values at or above the cohort median (0.0789, approximately 7.89% of sectors) were classified as high burden ($n = 18$); those below the median were

classified as lower burden (n = 17). Continuous fibrosis and the location of fibrotic regions were examined in supportive analyses.

For descriptive partitioning of fibrosis across territories, continuous whole-wall fibrosis percentages were summed over sectors and mice. The outside-scar contribution was calculated as the sum in border and remote sectors divided by the corresponding sum across all sectors. Sectors were equally weighted, without additional weighting by myocardial tissue area or wall thickness.

Physiologically summarized mechanical descriptors

Regional curves were converted into descriptors of waveform magnitude, extrema, timing, systolic and diastolic behavior and area under the curve. Dispersion descriptors summarized variation across cycles or myocardial regions. Relational descriptors quantified local differences, correlations, similarity and heterogeneity between neighboring regions. Features were summarized separately within scar, border and remote myocardium; the primary regional representation retained border, remote and border-minus-remote information in one vector per mouse. A comparator representation averaged the same mechanical information across the complete short-axis view.

Principal-component analysis was fitted only to D5 regions from the four sham hearts after outcome-independent feature refinement; infarcted regions were then projected into this fixed space. Regional mechanical similarity networks were constructed from a nonredundant set of descriptors without using D30 fibrosis to select features, position nodes or define edges. These analyses visualized the mechanical space and were not used to estimate predictive performance.

Regional association and prediction

We evaluated associations between D5 descriptors and local D30 fibrosis within each mouse and then combined across animals, separately in scar, border and remote myocardium. Within-mouse Pearson correlations were Fisher-z transformed, averaged with equal weight across mice and back-transformed. Two-sided inference used sign-flipping of mouse-level coefficients, and confidence intervals used mouse-level bootstrap resampling. Benjamini-Hochberg correction was applied jointly across all 411 descriptors and three territories, rather than only to the descriptors displayed. These screens ranked local relationships and were not treated as independent region-level replication.

We evaluated regional prediction using leave-one-mouse-out outer validation: all regions from the held-out mouse were excluded from every fitting and feature-selection step. Logistic regression and a linear support-vector machine were fitted to summarized mechanics. The primary regional task concerned the 321 border-zone regions from all 35 mice; a matched analysis considered all 1,481 regions outside scar.

Mouse-level prediction from summarized mechanics

Primary mouse-level prediction used 35 outer leave-one-mouse-out folds and stratified five-fold inner cross-validation within each outer training set. Descriptors were ranked by their univariate ANOVA F statistic within each inner training fold. The number of selected descriptors was tuned over 1, 3, 5 and 10, and the logistic-regression inverse regularization parameter C over 0.05, 0.2 and 1.0, using mean inner-fold ROC-AUC. Class-balanced L2-penalized logistic regression was fitted after median imputation and standardization. The regional representation comprised mean descriptor values in border and remote myocardium and their border-minus-remote differences. The global representation comprised descriptor means and standard deviations across all 48 short-axis sectors. Both models included D5 mechanically defined scar fraction as a mandatory covariate; feature-number selection applied only to the additional mechanical descriptors. To explore incremental information, a cross-fitted regional-mechanics score was added to a reference model containing D5 mechanically defined scar fraction, ejection fraction and global circumferential strain. A second reference analysis replaced global circumferential strain with GLS. All score construction and model fitting were repeated within each outer training set before application to the held-out mouse.

The effect of spatial organization was examined by circularly shifting or freely permuting sector-to-territory correspondence and repeating the complete analysis. The relationship between the cross-fitted regional score and the continuous fibrosis fraction outside scar was evaluated as a supportive analysis. Leave-one-cohort-out validation assessed transportability and was kept separate from the primary leave-one-mouse-out estimate.

Prediction from complete deformation signals

We analyzed complete D5 deformation signals at regional and mouse level as a benchmark against physiologically summarized mechanics. MiniROCKET captured time-series patterns through fixed convolutional transforms [17]. Compact convolutional neural networks learned local waveform features

[15]. Graph models represented the 48-region myocardial circumference as neighboring nodes [16]. At mouse level, global and territory-aware pooling strategies were evaluated for the convolutional models; N-way partial least squares was added after inspection of the initial analyses and is reported as a post-hoc benchmark.

The regional comparison used the same mice, territories, fibrosis labels and leave-one-mouse-out partitions as the summarized-mechanics analysis. Regions outside the target territory were omitted from the fitting loss and evaluation, while the complete 48-region signal tensor and territory indicators remained available to the tensor models. At mouse level, all approaches used the same 35 mice, the same high-fibrosis outcome and the same outer partitions. MiniROCKET and convolutional predictions were averaged across three fixed random seeds (11, 29 and 47); no seed was selected according to performance.

Whole-heart spatial-resolution sensitivity analysis

Three independent hearts underwent D5 four-dimensional echocardiography and D30 whole-mount Alcian Blue and high-resolution episcopic microscopy. After echography, left-ventricular endocardial and epicardial contours were segmented across the cardiac cycle using a customized 4D Strain Toolbox (10.5281/zenodo.23452768), with the eight longitudinal levels spanning from apical (0.48 mm) to basal (3.84 mm) planes. These eight longitudinal levels along with the 48 circumferential sectors, yield 384 spatial cells per heart. Sector 1 lay immediately to the left of the superior meridian, sector 48 immediately to its right, and numbering proceeded counterclockwise. Correspondence between imaging and tissue maps was established anatomically from the septal insertion landmark and recorded heart orientation.

At each level, scar was defined from within-heart normalized D5 radial strain using the 0.10 threshold. The whole-heart border neighborhood incorporated circumferential neighbors and the corresponding region at adjacent longitudinal levels; all other non-scar cells were remote. D30 fibrosis was analyzed continuously and as a binary outcome using a 10% regional threshold.

Unlike the 2D short-axis analysis which evaluated in-plane radial and circumferential strains, 4D volumetric tracking allowed deriving four deformation components: radial (wall thickening), circumferential (circular shortening), longitudinal (base-to-apex shortening across levels), and surface area strain (fractional change in local endocardial surface area). Prediction in border and remote cells combined these four metrics in leave-one-heart-out ridge models. Preprocessing and fitting were restricted to the training hearts. A sensitivity model standardized each strain variable within heart and longitudinal level to

reduce broad longitudinal gradients. Associations were also evaluated after centering ranks within longitudinal level. The three hearts, rather than individual spatial cells, were the independent biological units; this analysis was a spatial-resolution sensitivity analysis, not independent validation.

Spatial transcriptomics and Angptl2 analyses

D30 left-ventricular sections from nine infarcted and two sham hearts were profiled by spatial transcriptomics. Histological morphology, low-dimensional embeddings, transcriptional clusters and marker profiles were used to annotate myocardial tissue states. Spatial observations were assigned to the same anatomical coordinate system as regional mechanics and histology.

An exploratory transcriptome-wide screen related D30 spatial gene expression to summarized mechanical descriptors at D0, D5 and D30. At D5, 13,753 transcripts were tested against 480 descriptors. Benjamini-Hochberg adjustment was applied across all gene–descriptor comparisons within each time point. This multiplicity correction did not account for dependence among spatial observations from the same heart, and the pooled screen was therefore used to nominate candidate genes. *Angptl2* was subsequently evaluated in exploratory analyses relating its expression to histological fibrosis, extracellular-matrix genes and predefined cellular gene-expression signatures. Region- and layer-adjusted rank correlations were calculated within each heart and combined across hearts using sign-flip inference and heart-level bootstrap confidence intervals. In these follow-up analyses, the heart was the unit of inference. Mixed-cell spots were not used to assign *Angptl2* to an exclusive cellular source.

Exploratory prediction of D30 Angptl2 expression from D5 summarized mechanics used nested leave-one-heart-out ridge regression. Imputation, scaling, feature ranking and regularization tuning were repeated within the training hearts. Robustness was assessed by rebuilding the procedure after exclusion of each heart and by restricting the all-but-scar analysis to the nine infarcted hearts.

Statistical analysis

The mouse was the unit of inference for the short-axis study and the heart for whole-heart and transcriptomic analyses. Regional observations from the same biological unit were kept together. The mouse was the unit of inference for the short-axis study and the heart for whole-heart and transcriptomic analyses. Regional observations from the same biological unit were kept together. Receiver operating characteristic area under the curve (ROC-AUC) was calculated from held-out predictions. The paired

regional-versus-global AUC comparison used 100,000 mouse-level bootstrap resamples and 200,000 score swaps. Exploratory incremental-value comparisons used 10,000 bootstrap resamples and 20,000 score swaps. These procedures used fixed out-of-fold predictions; preprocessing, feature selection, hyperparameter tuning and model fitting were not repeated during resampling or score swapping. The resulting intervals and tests are therefore conditional on the generated predictions and do not capture the full uncertainty associated with model development. Correlations are reported as Pearson r or Spearman rho according to the specified analysis. Benjamini-Hochberg-adjusted values are reported as q values. All tests were two-sided unless explicitly stated. Primary, exploratory and sensitivity analyses were interpreted separately, and no causal inference was made from association or prediction.

Custom analysis code was developed with assistance from Codex (OpenAI). All analytical decisions, code outputs, figures and interpretations were reviewed by the authors.

Results

Early myocardial dysfunction is followed by heterogeneous fibrosis outside the scar

We measured regional myocardial mechanics five days after permanent coronary ligation, and ventricular remodeling and we assessed fibrosis at day 30 (D30; Fig. 1a). The primary analysis included 35 infarcted mice from three experimental cohorts (3 experimenters from 2 laboratories); four sham-operated mice provided descriptive controls. The myocardial circumference was divided into 48 regions. Regional radial strain over the cardiac cycle defined the most mechanically impaired territory at D5, designated scar, its surrounding border zone, and remote myocardium independently of D30 histology (Fig. 1c,d).

Late ventricular remodeling varied substantially between animals. To characterize this heterogeneity, we classified the infarcted mice with available D30 echocardiography according to global longitudinal strain (GLS), a measure of ventricular shortening. Using a cutoff of -9%, 16 mice showed an adaptive phenotype (GLS < -9%), whereas 16 showed a heart failure-like phenotype with more severely impaired longitudinal contraction (GLS ≥ -9%). This functional distinction was accompanied by marked differences in ventricular structure and pump function: median end-diastolic volume was 138.2 versus 56.7 µL, and median ejection fraction was 22.5% versus 50.7%, in heart failure-like versus adaptive mice, respectively. Both differences persisted after adjustment for experimental cohort ($P < 0.001$ for each; Fig. 1b and Supplementary Fig. S1).

D5 territory extent was similar between phenotypes, whereas D30 fibrosis was greater in scar and border-

zone myocardium in heart failure-like mice (cohort-adjusted nominal P = 0.0100 and P = 0.00159, respectively; Fig. 1e–g).

At D30, fibrosis was densest within the scar but extended variably into border-zone and remote myocardium. Across all 35 infarcted mice, the median of the within-mouse mean fibrosis percentages was 14.5% in the scar, 6.5% in the border zone, and 0.99% in remote myocardium. Border and remote myocardium comprised 88.2% of mapped sectors and together contained 62.0% of the fibrosis signal summed across sectors. D5 scar extent showed no detectable association with the subsequent fraction of fibrotic sectors outside scar (Spearman rho = 0.064, P = 0.72; Fig. 1h). We therefore examined whether regional mechanical behavior could identify hearts that would develop more extensive fibrosis in the surviving myocardium.

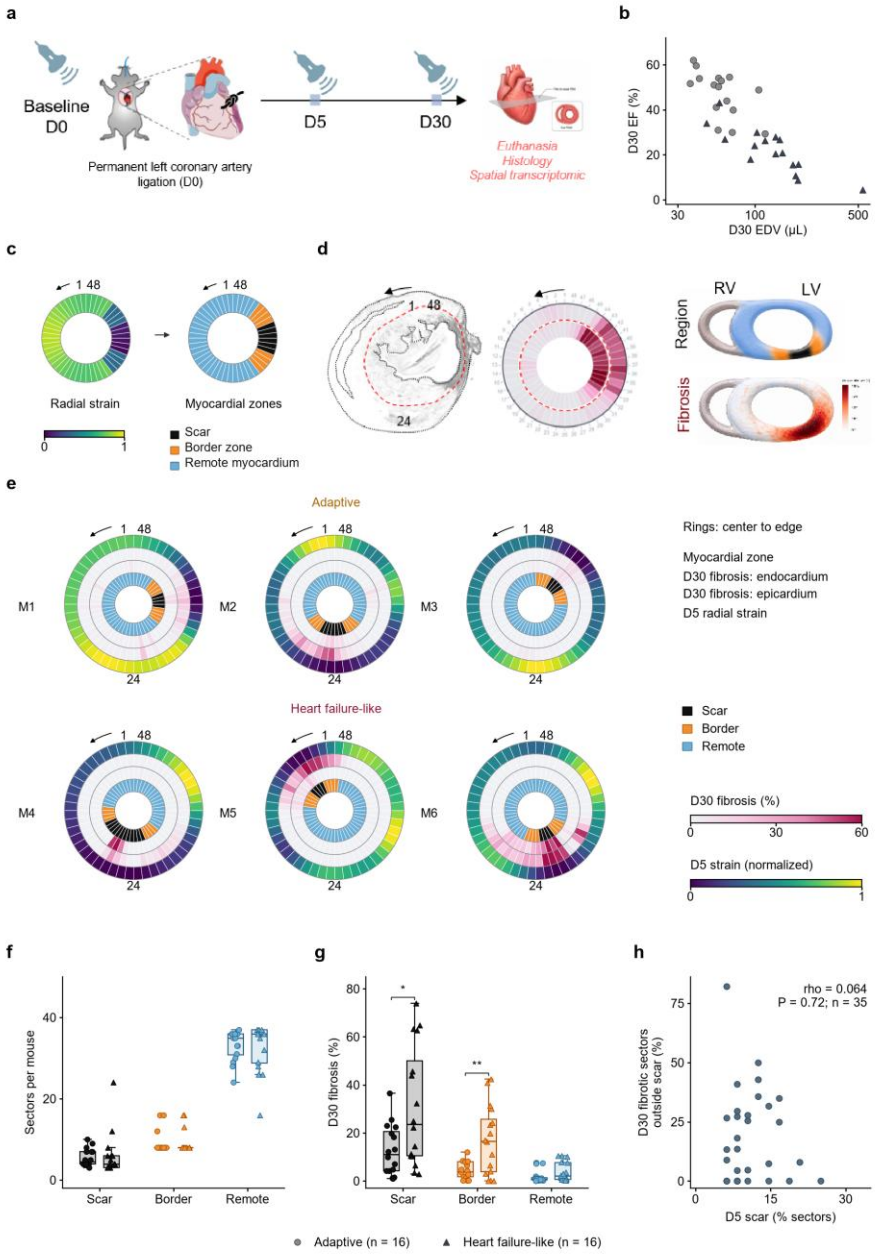

Figure 1: Early myocardial dysfunction and heterogeneous late remodeling after infarction

a, Experimental timeline: echocardiography at baseline (D0), D5 and D30 after permanent coronary ligation, followed by D30 histology and spatial transcriptomics. **b**, D30 end-diastolic volume (EDV; logarithmic scale) and ejection fraction (EF) in 32 infarcted mice. Adaptive and heart failure-like phenotypes were defined by D30 global longitudinal strain (GLS below -9% and GLS of -9% or greater; n = 16 each). Three mice without D30 GLS remained in the 35-mouse prediction cohort. **c**, D5 myocardial territories. The full-cycle radial-strain integral was normalized within each mouse; values <0.10 defined scar, four adjacent regions on either side defined the border zone, and the remainder remote myocardium. **d**, Anatomical correspondence of regional mechanics and D30 fibrosis; supplied anatomical images are schematic. **e**, Six representative mice. Rings show, from centre to periphery, D5 territory, D30 endocardial fibrosis, D30 epicardial fibrosis and normalized D5 radial strain. Numbering proceeds counterclockwise. **f,g**, D5 territory extent (f) and within-mouse mean D30 fibrosis (g) in the 32 phenotype-classified mice. Circles denote adaptive and triangles heart failure-like remodeling. Boxes show median and interquartile range; whiskers extend to 1.5 times the interquartile range. Cohort-adjusted two-sided P values for scar, border and remote regions were 0.892, 0.773 and 0.931 in f, and 0.0100, 0.00159 and 0.0777 in g. Asterisks indicate nominal secondary comparisons: one, $P < 0.05$; two, $P < 0.01$. **h**, D5 scar extent and the fraction of D30 fibrotic regions outside scar in all 35 infarcted mice; two-sided Spearman correlation. Border and remote myocardium comprised 88.2% of mapped regions and 62.0% of sector-integrated D30 fibrosis burden.

Regional mechanics anticipate later fibrosis outside scar

Regional deformation curves were summarized using features describing the magnitude and timing of motion, variability, and relationships between neighboring myocardial regions (Fig. 2). These descriptors were organized by D5 myocardial territory to preserve differences between border-zone and remote mechanics. We tested whether this regional profile identified mice with a high D30 fibrosis burden outside the scar, defined from the fraction of fibrotic sectors in the combined border and remote territories.

We first examined prediction at the level of individual myocardial regions. Dimension-reduced maps and mechanical similarity networks illustrated regional heterogeneity onto which D30 fibrosis mapped unevenly. In analyses that accounted for observations originating from the same mouse, the largest local correlations involved border-zone radial mechanics, although none remained significant after correction for multiple comparisons. Multivariable models based on summarized D5 mechanics nevertheless discriminated fibrotic from non-fibrotic border-zone regions. Across 321 regions from 35 mice, with all regions from each held-out mouse excluded together, the area under the receiver operating characteristic curve (ROC-AUC) was 0.671 for logistic regression and 0.687 for a linear support-vector machine (Fig. 2). Thus, the regional analysis addressed where fibrosis subsequently developed while preserving the mouse as the unit of validation.

When each of the 35 mice was held out in turn, regional mechanics yielded a ROC-AUC of 0.732 (95% CI, 0.546–0.885). Averaging mechanical information across the complete short-axis view yielded a ROC-AUC of 0.513. The paired difference was 0.219 (95% mouse-level bootstrap CI, −0.003 to 0.441; P = 0.064). Regional discrimination was therefore numerically higher, although the uncertainty in the direct comparison included no difference (Fig. 2).

Regional mechanics add information to the tested reference models

We next conducted an exploratory analysis to assess whether the regional score added predictive information to reference models comprising early measures of injury and ventricular function. A reference model comprising D5 mechanically defined scar fraction, ejection fraction and global circumferential strain yielded a ROC-AUC of 0.454. Adding the regional-mechanics score increased the ROC-AUC to 0.683 (paired difference, 0.229; 95% mouse-level bootstrap CI, 0.086-0.392; P = 0.0015; Fig. 2). All steps used to

construct the regional score and fit the combined model were repeated using only the training animals before testing each held-out mouse.

We also observed an increase when global circumferential strain was replaced by global longitudinal strain (AUC, 0.546 to 0.657; paired difference, 0.111; 95% CI, 0.020-0.224). The regional score alone retained the highest observed AUC (0.732), compared with 0.683 and 0.657 for the combined GCS- and GLS-based models, respectively. These exploratory analyses support added predictive information relative to the reference models tested, while the benefit of combining conventional measurements with the regional score remains to be established (Supplementary Fig. S3).

To examine the contribution of location, we disrupted the correspondence between regional mechanics and the D5 territory map and repeated the complete prediction procedure. Mean AUC decreased to 0.544 after circular shifts and to 0.566 after unrestricted sector permutation, compared with the observed value of 0.732. Neither comparison reached the 0.05 significance threshold ($P = 0.100$ and $P = 0.130$, respectively). Thus, disturbing regional localization lowered average performance, but these tests did not establish that the exact circumferential arrangement was responsible for the observed regional advantage (Supplementary Fig. S3).

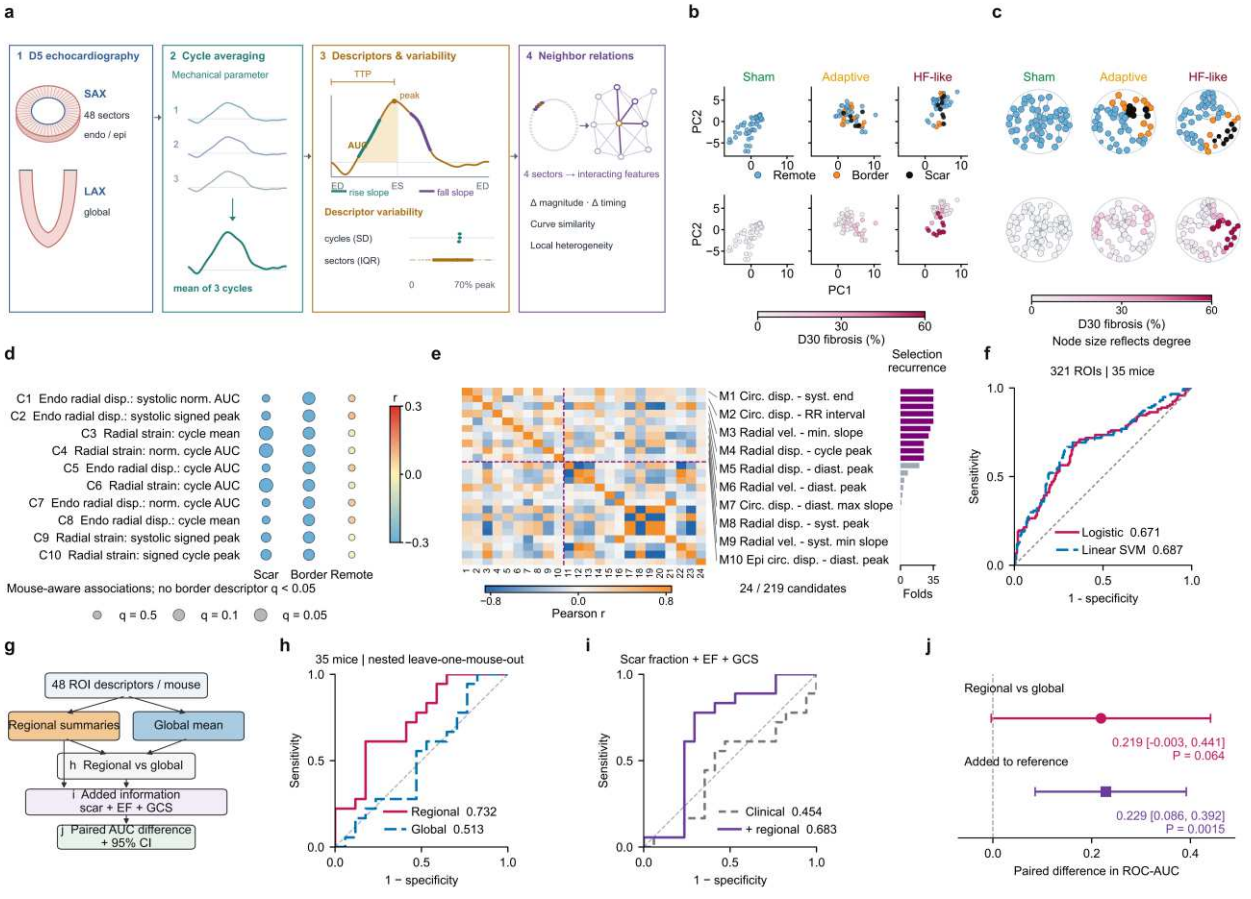

Figure 2: Regional mechanical organization anticipates subsequent fibrosis

a, Derivation of descriptors of waveform magnitude and timing, variability and relationships between neighboring regions. **b**, Representative D5 regions projected into a principal-component space fitted on four sham mice. **c**, Mechanical similarity networks in representative sham, adaptive and heart failure-like hearts. In b,c, upper plots show D5 territories and lower plots show the same observations recolored by D30 fibrosis; fibrosis was not used to position observations or construct networks. **d**, Mouse-aware associations between D5 descriptors and local D30 fibrosis. Color shows within-mouse correlation and bubble area adjusted statistical evidence; no border-zone descriptor reached q < 0.05 after correction. **e**, Correlation and selection recurrence among regional candidates. The heatmap shows 24 of 219 candidates; M1-M10 are the ten most frequently selected across 35 outer folds. **f**, Prediction of fibrosis in 321 border-zone regions from 35 mice, leaving out all regions from one mouse together. ROC-AUC was 0.671 for logistic regression and 0.687 for linear support-vector classification. **g**, Mouse-level analysis: regional and global representations were compared in h; the cross-fitted regional score was added to scar fraction, EF and global circumferential strain (GCS) in i; paired AUC differences are summarized in j. All processing was repeated within each outer fold. **h**, Held-out ROC curves for high D30 fibrosis burden outside scar from regional or globally averaged mechanics (AUC, 0.732 and 0.513). **i**, Reference model comprising scar fraction, EF and GCS, before and after adding the regional score (AUC, 0.454 and 0.683). **j**, Paired AUC differences with mouse-bootstrap 95% confidence intervals and two-sided score-swap P values: regional versus global, 0.219 (-0.003 to 0.441), P = 0.064; reference plus regional score versus reference, 0.229 (0.086 to 0.392), P = 0.0015. AUC, area under the curve; ROC, receiver operating characteristic.

Whole-heart mapping extends the analysis across ventricular levels

The regional framework was extended to three hearts with whole-heart echocardiography and D30 fibrosis mapping across eight longitudinal levels, each comprising 48 circumferential sectors. In this spatial-resolution sensitivity analysis, while radial strain showed the strongest association with fibrosis after level adjustment (Spearman rho = -0.300, q = 0.016), area and circumferential strain also showed consistent

negative trends across levels, as shown in Supplementary Fig. S4e. A model combining four strain measurements yielded a pooled leave-one-heart-out ROC-AUC of 0.787 in border and remote myocardium. This decreased to 0.584 after removing broad differences between hearts and ventricular levels. Part of the whole-heart predictive signal therefore reflected longitudinal gradients. These observations extend the mapping approach beyond a single short-axis plane; the three hearts remained the independent biological units.

Summarized mechanics show higher observed discrimination than complete deformation signals

We next asked whether retaining the complete D5 deformation curves improved prediction compared with using physiological summaries of those curves (Fig. 3a,b). At the regional level, both representations were evaluated using the same mice, myocardial regions, fibrosis labels and held-out-mouse partitions. In the border zone, the best observed ROC-AUC was 0.687 for summarized mechanics and 0.510 for models trained directly on the complete signals. Across all myocardium outside scar, the corresponding values were 0.627 and 0.580 (Fig. 3c). This comparison therefore addressed the same local question—where fibrosis later developed—without excluding any mouse. Results for each individual model are reported in Supplementary Fig. S5.

We then compared the two representations at mouse level, using the same 35 mice, the same fibrosis outcome and the same held-out animals (Fig. 3d–g). The direct-signal approaches included methods that detect temporal patterns, learn local waveform features or reduce the complete multidimensional signal. The best observed ROC-AUC among these approaches was 0.556, obtained with MiniROCKET, compared with 0.732 for summarized regional mechanics. The paired difference was 0.176 (95% mouse-level bootstrap CI, −0.075 to 0.420). Other representations of the complete signals yielded ROC-AUCs between 0.343 and 0.526 (Supplementary Fig. S5).

Summarized regional mechanics therefore showed higher observed discrimination in both regional and mouse-level comparisons. Uncertainty around the direct mouse-level difference remained substantial, and these results do not establish that cohort size caused the lower performance of the complete-signal models. Rather, they show that physiologically interpretable summaries provided a more effective representation in this 35-mouse dataset.

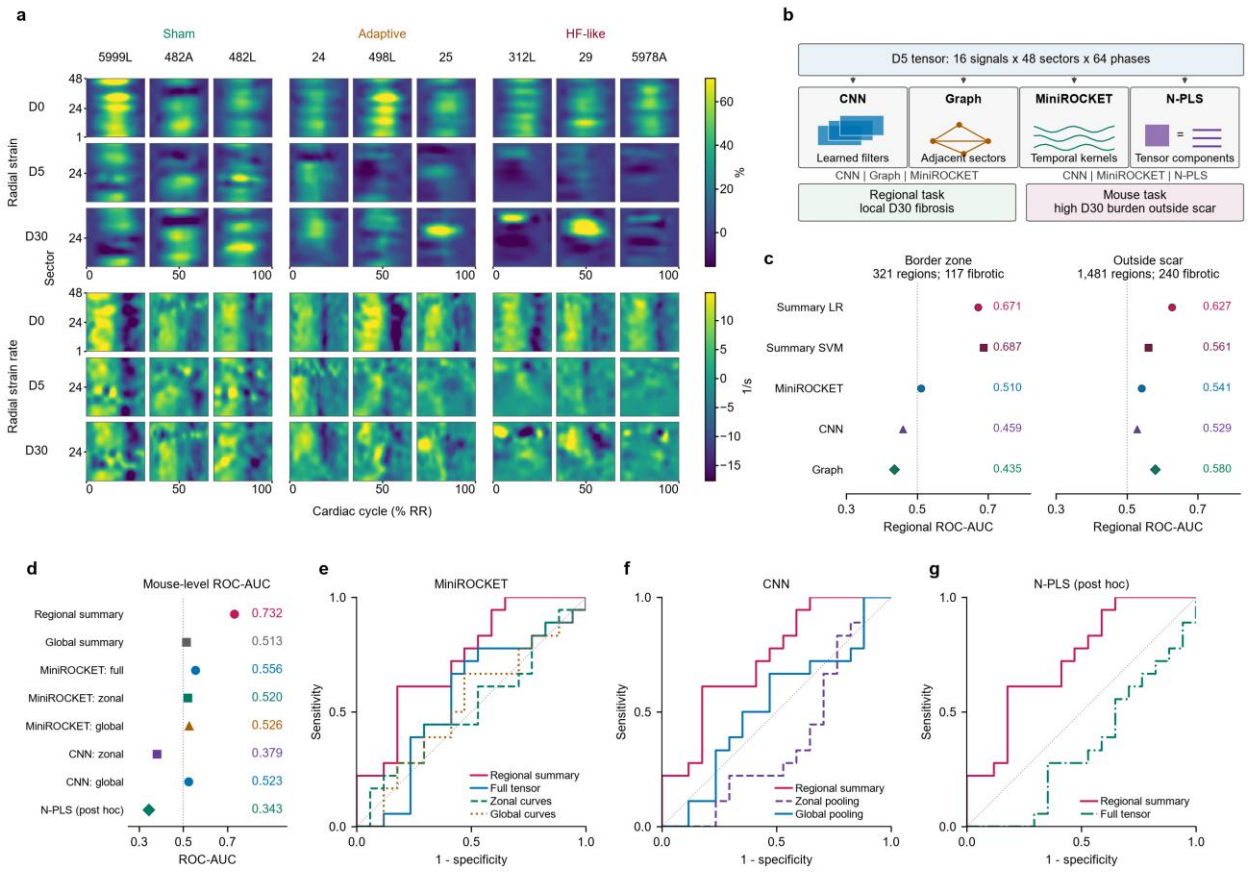

Figure 3: Physiological summaries and complete deformation signals provide complementary representations

a, Regional radial strain and strain rate at D0, D5 and D30 in nine illustrative mice. Each map contains 48 short-axis regions; only D5 signals were used for prediction. **b**, Complete-signal strategies and prediction tasks. CNN, Graph and MiniROCKET models predicted local D30 fibrosis; separately trained CNN, MiniROCKET and N-way partial least-squares (N-PLS) models predicted high mouse-level fibrosis burden outside scar. N-PLS was a post-hoc benchmark. Up to three cardiac cycles were averaged; a single available cycle was retained. **c**, Regional prediction using identical mice, territories, labels and leave-one-mouse-out folds. In 321 border-zone regions, AUCs were 0.671 and 0.687 for summarized-mechanics logistic regression and linear support-vector classification, versus 0.510, 0.459 and 0.435 for complete-signal MiniROCKET, CNN and Graph models. Across 1,481 regions outside scar, corresponding AUCs were 0.627, 0.561, 0.541, 0.529 and 0.580. **d**, Mouse-level discrimination for the same 35 infarcted mice (18 high and 17 low burden) and outer folds. Points are AUCs from held-out predictions. **e-g**, ROC curves comparing summarized regional mechanics with MiniROCKET (e), CNN pooling strategies (f) and N-PLS (g). MiniROCKET and CNN predictions were averaged across fixed seeds 11, 29 and 47. Summarized regional mechanics yielded AUC 0.732 versus 0.556 for complete-tensor MiniROCKET; paired difference, 0.176 (95% mouse-bootstrap confidence interval, -0.075 to 0.420). AUC, area under the curve; CNN, convolutional neural network; ROC, receiver operating characteristic.

Spatial transcriptomics identifies an Angptl2-associated matrix-remodeling state

Spatial transcriptomics at D30 characterized myocardial states in nine infarcted and two sham hearts (Fig. 4a–d). Tissue-state mapping separated remote, border and scar-associated transcriptional profiles, while Col1a1 expression and marker-gene patterns localized the matrix-remodeling component of this organization (Fig. 4c,d). Among the genes linked to regional mechanics, *Angptl2* emerged as a candidate associated with the D5 mechanical state (Fig. 4e). It showed the strongest single association after correction

for multiple testing among 13,753 transcripts. Because the pooled screen did not account for dependence among observations from the same heart, multiplicity-adjusted associations were used to nominate candidate genes. Subsequent analyses accounting for the heart as the biological unit were also considered exploratory and used the same heart series.

Immunofluorescence revealed a heterogeneous distribution of ANGPTL2 across the infarcted myocardium in overview and higher-magnification images (Fig. 4f). Across three hearts, the mean image-derived spatial profile showed greater ANGPTL2 signal in the border zone than in scar or remote myocardium, with variation between hearts (Fig. 4g). *Angptl2*-associated transcriptional profiles included extracellular-matrix and tissue-remodeling genes (Fig. 4h). Spatial maps illustrated *Angptl2* with *Col1a1* or *Gsn* in one sham and two infarcted hearts (Fig. 4i). Cellular-signature analysis showed the strongest associations with fibroblast and myofibroblast programs, with smaller mural/perivascular components (Fig. 4j). *Angptl2* expression was also associated with local histological fibrosis in remote myocardium and across myocardium outside scar (Supplementary Fig. S6). Together, these findings place *Angptl2* within a matrix-remodeling tissue state, while the mixed-cell composition of transcriptomic spots precludes assignment to an exclusive cellular source.

Exploratory prediction analyses related D5 mechanics to D30 Angptl2 expression across myocardium outside scar in the complete 11-heart series (rho = 0.664). However, the association was not retained after rebuilding the model in the nine infarcted hearts alone (rho = 0.100, P = 0.798), and border-zone predictions were sensitive to individual-heart removal. The molecular findings therefore provide a biological context for post-infarction remodeling rather than independent confirmation of the fibrosis-prediction result (Supplementary Fig. S6).

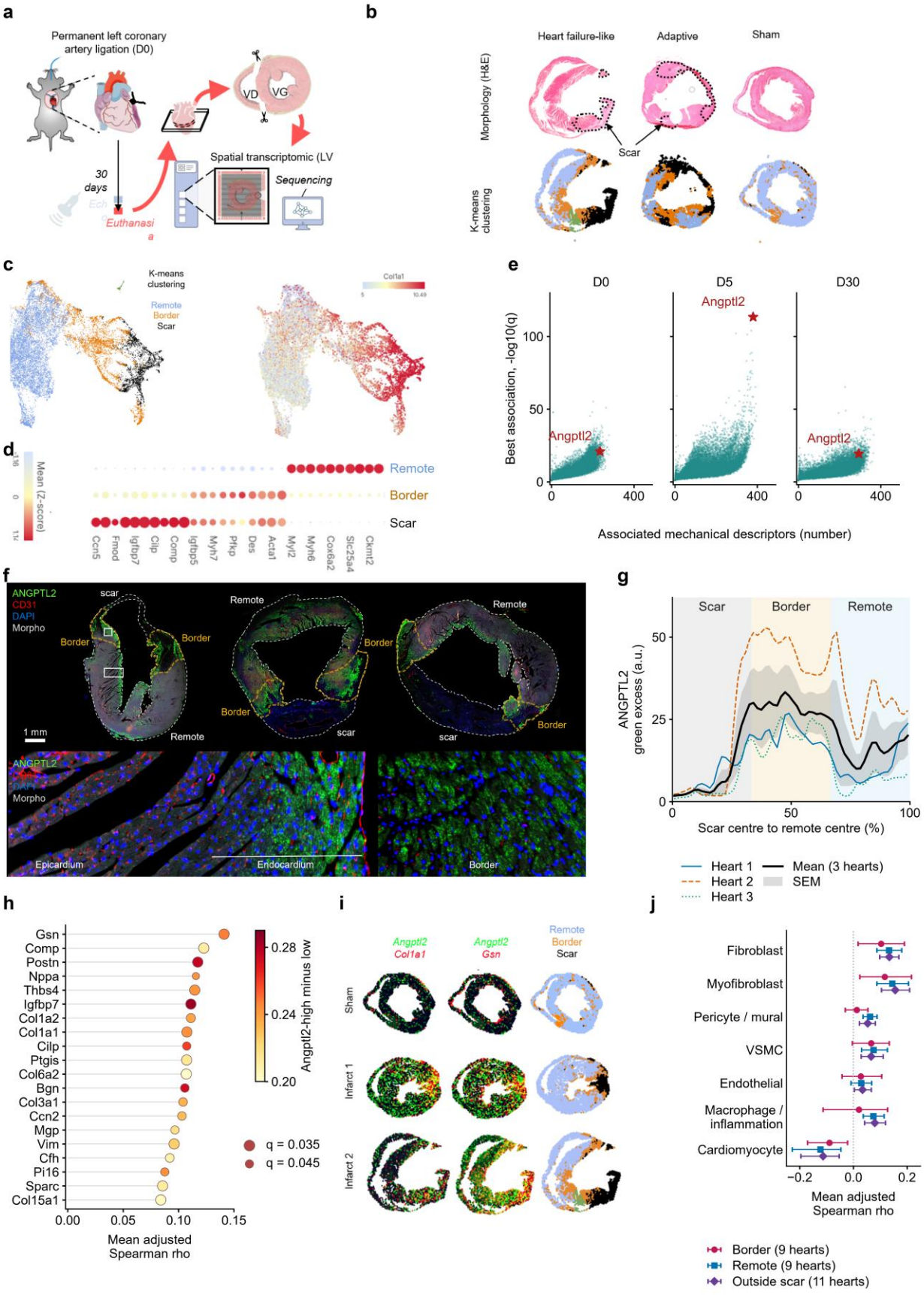
a
Permanent left coronary artery ligation (D0)
VD
VG
30 days
Echo
Euthanasia
Spatial transcriptomic (LV
Sequencing
b
Heart failure-like
Adaptive
Sham
Morphology (H&E)
K-means clustering
Scar
c
K-means clustering
Remote
Border
Scar
Col1a1
d
Mean (z-score)
Remote
Border
Scar
Ccn5
Fmod
Igfbp7
Cilp
Comp
Igfbp5
Myh7
Pfkp
Des
Acta1
Myl2
Myh6
Cox6a2
Slc25a4
Ckmt2
e
D0
D5
D30
Angptl2
Best association, -log10(q)
Associated mechanical descriptors (number)
f
ANGPTL2
CD31
DAPI
Morpho
scar
Border
Remote
1 mm
Epicardium
Endocardium
g
Scar
Border
Remote
ANGPTL2 green excess (a.u.)
Scar centre to remote centre (%)
Heart 1
Heart 2
Heart 3
Mean (3 hearts)
SEM
h
Gsn
Comp
Postn
Nppa
Thbs4
Igfbp7
Col1a2
Col1a1
Cilp
Ptgis
Col6a2
Bgn
Col3a1
Ccn2
Mgp
Vim
Cfh
Pi16
Sparc
Col15a1
Angptl2-high minus low
q = 0.035
q = 0.045
Mean adjusted Spearman rho
i
Angptl2 Col1a1
Angptl2 Gsn
Remote
Border
Scar
Sham
Infarct 1
Infarct 2
j
Fibroblast
Myofibroblast
Pericyte / mural
VSMC
Endothelial
Macrophage / inflammation
Cardiomyocyte
Mean adjusted Spearman rho
Border (9 hearts)
Remote (9 hearts)
Outside scar (11 hearts)

440

Figure 4 | Spatial transcriptomics identifies an Angptl2-associated matrix-remodeling state after myocardial infarction

a, D30 spatial-transcriptomic workflow; nine infarcted and two sham hearts. **b**, Morphology and tissue-state maps in heart failure-like, adaptive and sham hearts. **c**, UMAPs colored by tissue state (left) or Col1a1 expression (right). **d**, Marker-gene expression across remote, border and scar states; color represents mean standardized expression. **e**, Exploratory associations between D30 gene expression and summarized mechanics at D0, D5 or D30. Points represent transcripts; axes show the number of associated descriptors at Benjamini–Hochberg $q < 0.05$ and the strongest adjusted association. Among 13,753 transcripts screened against 480 D5 descriptors, Angptl2 showed the strongest adjusted association and was associated with 379 descriptors. This pooled screen nominated candidates but did not resolve within-heart dependence. **f**, Immunofluorescence in three post-infarction hearts showing ANGPTL2 (green), CD31 (red) and DAPI (blue). Scar, border and remote myocardium are annotated. Overview scale bar, 1 mm. Lower images show epicardial, endocardial and border areas from the first heart. **g**, Descriptive image-derived ANGPTL2 profiles. Colored lines identify hearts; black line and gray band show mean and SEM (n = 3). Territories were assigned equal normalized widths and both wall sides were averaged within heart. Position is normalized. **h**, Twenty transcripts with the largest Angptl2-high versus low effects among genes associated with Angptl2 at transcriptome-wide $q < 0.05$. Position, color and bubble area represent mean within-heart Spearman correlation adjusted for state and layer, high-minus-low effect and q, respectively. Associations were combined across 11 hearts. **i**, Spatial Angptl2 (green) with Col1a1 or Gsn (red), and tissue-state maps, in one sham and two infarcted hearts. Patterns do not establish single-cell colocalization. **j**, Angptl2 associations with cellular expression signatures adjusted for state and layer. Points show mean within-heart Spearman correlations; bars show heart-bootstrap 95% confidence intervals. Border and remote analyses included nine infarcted hearts; myocardium outside scar included all 11 hearts. Fibroblast and myofibroblast programs showed the strongest positive associations, with smaller mural/perivascular components.

Discussion

This study addresses a simple question using a spatial design: can early kinematic patterns after myocardial infarction be used to identify hearts that later develop fibrosis beyond the replacement scar? Three findings support this possibility. First, late fibrosis was not confined to the most mechanically impaired territory; border and remote myocardium together contained 62% of the sector-integrated fibrosis signal. Second, regional mechanics showed higher observed discrimination than global averaging (ROC-AUC, 0.732 versus 0.513). Its cross-fitted score also added information to early scar extent, ejection fraction and global strain. Third, spatial transcriptomics placed the imaging phenotype within a later matrix-remodeling state enriched for fibroblast and myofibroblast programs.

The distinction between replacement scar and fibrosis in surviving myocardium is central to the interpretation. Matrix deposition within the infarct replaces lost cardiomyocytes and is mandatory to maintain ventricular integrity [6,7]. Fibrosis beyond the scar has a different biological and clinical meaning because it affects nonischemic myocardium expected to sustain ventricular function. Experimental work has shown widespread fibroblast activation with spatially restricted collagen accumulation after infarction [8], and remote myocardial fibrosis in patients is associated with heart-failure events and mortality while relating only weakly to infarct size [9]. Our findings add an early functional dimension: myocardium that later becomes fibrotic already participates in an abnormal regional mechanical pattern five days after injury.

The main result is not a single strain threshold or one isolated feature. It is the organization of multiple mechanical characteristics across related myocardial territories. Regional deformation and dyssynchrony are known to capture prognostic information beyond conventional global measurements after infarction [2–5]. In exploratory analyses, adding the regional score improved discrimination relative to the two reference models tested. Both combined models had lower observed AUCs than the regional score alone, leaving the value of combining these measurements to be established in independent cohorts. The regional representation achieved higher observed discrimination than globally averaged mechanics, although the paired difference remained uncertain (difference in ROC-AUC, 0.219; 95% confidence interval, -0.003 to 0.441; P = 0.064). Similarly, spatial perturbation lowered average performance but did not reach conventional significance. These results therefore support a regional signal without proving that one exact circumferential arrangement is uniquely responsible for it.

Comparing complete deformation signals and physiological summaries helps clarify how this signal can be used in a modest experimental cohort. Raw curves contain rich temporal and spatial information, but they also create a high-dimensional learning problem. Models trained directly on the complete signals showed lower observed discrimination than summarized regional mechanics on matched regional and mouse-level tasks. This does not establish that summary features are universally superior or that cohort size alone caused the difference. It indicates that, in these 35 mice, physiologically constrained summaries provided an efficient and interpretable representation of the available information. Such representations may be especially useful when biological sample size is limited but regional sampling is dense.

The whole-heart analysis extended the mapping framework from one mid-ventricular plane to eight longitudinal levels. The raw four-strain model retained an observed relationship with D30 fibrosis, but performance decreased after removing broad differences between hearts and ventricular levels. This drop in performance after level-standardization is biologically expected, because physiological base-to-apex wall stress gradients naturally vary along the ventricle, rather than being simply measurement noise. Longitudinal anatomy therefore contributed materially to the raw signal. The residual inverse association between radial strain and fibrosis supports a local component, while the three-heart sample requires this result to remain a sensitivity analysis rather than external validation.

Spatial transcriptomics provided biological context rather than a second validation cohort. Angptl2 emerged from an exploratory screen and localized within a broader matrix-remodeling program. Its strongest

cellular-signature relationships involved fibroblast and myofibroblast programs, with a smaller mural/perivascular component. This is consistent with earlier evidence connecting ANGPTL2 to pathological cardiac remodeling [14], but the present data neither establish a causal role nor identify one exclusive cellular source. Moreover, mouse-level Angptl2 prediction was sensitive to cohort composition. The robust conclusion is therefore that early mechanics is associated with a later fibrovascular remodeling state in which Angptl2 is one candidate marker.

The translational implication is that early echocardiography may eventually contribute more than a global estimate of ventricular dysfunction. A regional mechanical map could help identify surviving myocardium at risk of later matrix remodeling, complementing measures of infarct extent and chamber function. Translation will require automated and standardized tracking, a clinically applicable reference for non-scar fibrosis, and validation in reperfused and heterogeneous human infarction. The present machine-learning models are analytical tools for testing this concept.

Limitations

This study provides a framework for linking early regional mechanics to subsequent myocardial fibrosis. Its predictive performance was evaluated in 35 infarcted mice from three experimental cohorts, using leave-one-mouse-out validation to keep all observations from each animal strictly separated between training and testing. Independent validation will be the next step in establishing generalizability, particularly given the performance differences observed across cohorts. For the AUC comparisons, bootstrap intervals and score-swap tests are conditional on fixed held-out predictions and do not encompass the full variability associated with feature selection, tuning and model fitting. The median-based binary endpoint enabled consistent comparisons between models within this dataset, although its cutoff does not represent a universal biological threshold. The continuous-outcome analysis provided complementary evidence, while its full-pipeline permutation test remained inconclusive.

Permanent coronary ligation enabled the study of remodeling after a sustained ischemic injury; extending this framework to reperfused infarction will help assess its relevance to contemporary clinical care. The D5 mechanical definition of scar and the four neighboring sectors on either side provided a consistent spatial framework across animals. These operational territories simplify the continuous transition from infarcted to surviving myocardium and do not quantify anatomical scar thickness. The precision of correspondence

between echocardiographic and tissue coordinates also remains an important determinant of cross-modal analyses. The 48-sector grid enabled consistent comparison with histology, but its sampling density should not be equated with independently resolved ultrasound measurements. Effective strain resolution depends on image acquisition and speckle-tracking processing, and neighboring sector estimates may share spatial information. Sector-level predictions should therefore be interpreted as regional localization rather than histological-scale delineation of fibrosis.

The comparisons between complete deformation signals and summarized descriptors provide benchmarks for this experimental setting, with substantial uncertainty remaining around their paired performance differences. The N-way partial least-squares model was an additional post-hoc benchmark. Whole-heart mapping extended the analysis across eight ventricular levels in three hearts, which remain the three independent biological replicates regardless of the number of sampled cells. Spatial transcriptomics in 11 hearts enabled candidate discovery through an initial pooled screen followed by analyses accounting for observations nested within hearts; larger datasets will strengthen the reproducibility of these associations. Finally, because transcriptomic spots contain mixtures of cells, complementary cellular localization and intervention studies will be needed to identify the cellular sources of Angptl2 and distinguish a functional contribution to fibrosis from its role as a marker of the remodeling state.

Conclusion

Early after myocardial infarction, the surviving ventricle carries a spatial mechanical signature of its later remodeling trajectory. Retaining regional organization showed promise for anticipating fibrosis outside the replacement scar and provided complementary information to the tested measures of injury and ventricular function. These findings provide an experimental framework for testing whether early regional echocardiographic mechanics can improve prediction of later fibrotic remodeling in patients after myocardial infarction. Prospective clinical validation will be required to establish its added value beyond conventional measures of injury and ventricular function. If confirmed, this approach could support more individualized follow-up and help identify patients for trials aimed at preventing adverse remodeling.

Declarations

Ethics approval

Animal procedures were authorized under APAFIS #39803-2022112915461850 and #43480-2022112915461850 by the Ministère de l'Enseignement supérieur et de la Recherche, Direction générale de la recherche et de l'innovation.

Data and code availability

Source data underlying the main and supplementary figures are provided with this article. The spatial transcriptomics datasets, the 4D strain-processing toolbox and scripts used for the whole-heart datasets, together with the code for data analysis and machine learning, are archived in a public repository under the following DOI: 10.5281/zenodo.23452768.

Funding, competing interests, author contributions and acknowledgements

This work was supported by Université Paris-Cité (Stratex RM27J23IDX91_S-FOREVER, and Stratex XM2725IPA034_TEMPOSHOCK) as well as the French National Research Agency (ANR) under grant ANR-25-CE14-2932-01 HyCaReS. This work was performed in collaboration with FRIM facility (UMS34), University of Paris Diderot, member of France Life Imaging (grant ANR-11-INBS-0006) and IDEX Imagerie Du Vivant networks, in collaboration with IAME group (UMR1137), and a Chateaubriand Fellowship (EGR).

Author Contributions

Conceptualization: A.N., G.C., G.F.

Methodology: N.P., T.D-M., Y.Y., M.P., E.G-R., L.M.G.

Investigation: N.P., T.D-M., V.S., M.P., S.M., E.G-R., L.M.G., P.S.

Writing - original draft: G.C., G.F.

Writing - review & editing: Y.Y., L.M.G., S.R., C.G., P.S., A.N., G.C., G.F.

Supervision: G.C., G.F.

References

1. Chareonthaitawee P, Christian TF, Hirose K, Gibbons RJ, Rumberger JA. Relation of initial infarct size to extent of left ventricular remodeling in the year after acute myocardial infarction. J Am Coll Cardiol. 1995;25:567–573. doi:10.1016/0735-1097(94)00431-O.

2. Reindl M, Tiller C, Holzknecht M, et al. Global longitudinal strain by feature tracking for optimized prediction of adverse remodeling after ST-elevation myocardial infarction. Clin Res Cardiol. 2021;110:61–71. doi:10.1007/s00392-020-01649-2.

3. Mollema SA, Liem SS, Suffoletto MS, et al. Left ventricular dyssynchrony acutely after myocardial infarction predicts left ventricular remodeling. J Am Coll Cardiol. 2007;50:1532–1540. doi:10.1016/j.jacc.2007.07.025.

4. Zhang Y, Yip GW, Chan AKY, et al. Left ventricular systolic dyssynchrony is a predictor of cardiac remodeling after myocardial infarction. Am Heart J. 2008;156:1124–1132. doi:10.1016/j.ahj.2008.07.019.

5. Wang N, Hung CL, Shin SH, et al.; VALIANT Investigators. Regional cardiac dysfunction and outcome in patients with left ventricular dysfunction, heart failure, or both after myocardial infarction. Eur Heart J. 2016;37:466–472. doi:10.1093/eurheartj/ehv558.

6. Fu X, Khalil H, Kanisicak O, et al. Specialized fibroblast differentiated states underlie scar formation in the infarcted mouse heart. J Clin Invest. 2018;128:2127–2143. doi:10.1172/JCI98215.

7. Chute M, Aujla PK, Qi Y, et al. ADAM15 is required for optimal collagen cross-linking and scar formation following myocardial infarction. Matrix Biol. 2022;105:127–143. doi:10.1016/j.matbio.2021.12.002.

8. Nagaraju CK, Dries E, Popovic N, et al. Global fibroblast activation throughout the left ventricle but localized fibrosis after myocardial infarction. Sci Rep. 2017;7:10801. doi:10.1038/s41598-017-09790-1.

9. Black N, Bradley J, Schelbert EB, et al. Remote myocardial fibrosis predicts adverse outcome in patients with myocardial infarction on clinical cardiovascular magnetic resonance imaging. J Cardiovasc Magn Reson. 2024;26:101064. doi:10.1016/j.jocmr.2024.101064.

10. Schuleri KH, Centola M, Evers KS, et al. Cardiovascular magnetic resonance characterization of peri-infarct zone remodeling following myocardial infarction. J Cardiovasc Magn Reson. 2012;14:24. doi:10.1186/1532-429X-14-24.

11. Calcagno DM, Taghdiri N, Ninh VK, et al. Single-cell and spatial transcriptomics of the infarcted heart define the dynamic onset of the border zone in response to mechanical destabilization. Nat Cardiovasc Res. 2022;1:1039–1055. doi:10.1038/s44161-022-00160-3.

12. Ninh VK, Calcagno DM, Yu JD, et al. Spatially clustered type I interferon responses at injury borderzones. Nature. 2024;633:174–181. doi:10.1038/s41586-024-07806-1.

13. Herum KM, Choppe J, Kumar A, Engler AJ, McCulloch AD. Mechanical regulation of cardiac fibroblast profibrotic phenotypes. Mol Biol Cell. 2017;28:1871–1882. doi:10.1091/mbc.E17-01-0014.

14. Tian Z, Miyata K, Kadomatsu T, et al. ANGPTL2 activity in cardiac pathologies accelerates heart failure by perturbing cardiac function and energy metabolism. Nat Commun. 2016;7:13016. doi:10.1038/ncomms13016.

15. LeCun Y, Bottou L, Bengio Y, Haffner P. Gradient-based learning applied to document recognition. Proc IEEE. 1998;86:2278–2324. doi:10.1109/5.726791.

16. Kipf TN, Welling M. Semi-supervised classification with graph convolutional networks. International Conference on Learning Representations. 2017. arXiv:1609.02907.

17. Dempster A, Schmidt DF, Webb GI. MiniROCKET: a very fast (almost) deterministic transform for time series classification. In: Proceedings of the 27th ACM SIGKDD Conference on Knowledge Discovery & Data Mining. 2021:248–257. doi:10.1145/3447548.3467231.

Supplementary Files

This is a list of supplementary files associated with this preprint. Click to download.

- STRAINV7.3SupplementaryFigurescorrected.pdf